

# Dynamin triple knockout cells reveal off target effects of commonly used dynamin inhibitors

Ryan J. Park<sup>1,2,3,4,5,\*</sup>, Hongying Shen<sup>1,2,3,4,5,\*</sup>, Lijuan Liu<sup>1,4,5</sup>, Xinran Liu<sup>1</sup>, Shawn M. Ferguson<sup>1,4,‡</sup> and Pietro De Camilli<sup>1,2,3,4,5,‡</sup>

<sup>1</sup>Department of Cell Biology, Yale University School of Medicine, New Haven, CT 06510, USA

<sup>2</sup>Department of Neurobiology, Yale University School of Medicine, New Haven, CT 06510, USA

<sup>3</sup>Howard Hughes Medical Institute, Yale University School of Medicine, New Haven, CT 06510, USA

<sup>4</sup>Program in Cellular Neuroscience, Neurodegeneration and Repair, Yale University School of Medicine, New Haven, CT 06510, USA

<sup>5</sup>Kavli Institute for Neuroscience, Yale University School of Medicine, New Haven, CT 06510, USA

\*These authors contributed equally to this work

‡Authors for correspondence ([pietro.decamilli@yale.edu](mailto:pietro.decamilli@yale.edu); [shawn.ferguson@yale.edu](mailto:shawn.ferguson@yale.edu))

Accepted 2 September 2013

Journal of Cell Science 126, 5305–5312

© 2013. Published by The Company of Biologists Ltd

doi: 10.1242/jcs.138578

## Summary

Dynamin, which is encoded by three genes in mammals, is a GTPase implicated in endocytic membrane fission. Dynamin 1 and 3 are predominantly expressed in brain, whereas dynamin 2 is ubiquitously expressed. With the goal of assessing the impact of the lack of dynamin on cell physiology, we previously generated and characterized dynamin 1 and 2 double knockout (DKO) fibroblasts. These DKO cells were unexpectedly viable in spite of a severe impairment of clathrin-mediated endocytosis. As low-level expression of the dynamin 3 gene in these cells could not be excluded, we have now engineered dynamin 1, 2 and 3 triple KO (TKO) fibroblasts. These cells did not reveal any additional defects beyond what was previously observed in DKO fibroblasts. Surprisingly, although fluid-phase endocytosis and peripheral membrane ruffling were not impaired by the lack of all three dynamins, two structurally similar, widely used dynamin inhibitors, dynasore and Dyngo-4a, robustly inhibited these two processes both in wild-type and TKO cells. Dynamin TKO cells will be useful tools for the further exploration of dynamin-dependent processes and the development of more specific dynamin inhibitors.

**Key words:** Dynamin, Dynasore, Dyngo, Actin, Synaptic vesicle, Synapse

## Introduction

Clathrin-mediated endocytosis is a very well-characterized process that functions in eukaryotes for the selective internalization of cell surface molecules and extracellular materials (Conner and Schmid, 2003; Doherty and McMahon, 2009; Kirchhausen, 2000; Robinson, 2004). In neurons, clathrin-mediated endocytosis is additionally implicated in neurotransmission because of its role in the endocytic recycling of synaptic vesicles at nerve terminals (Brodin et al., 2000; Dittman and Ryan, 2009; Heuser and Reese, 1973; Saheki and De Camilli, 2012).

Clathrin-mediated endocytosis is a highly coordinated process that begins with the assembly of clathrin coat components at the plasma membrane through interactions with plasma membrane lipids and with membrane proteins destined for internalization by this endocytic pathway. The nascent bud grows and invaginates with the assistance of multiple accessory factors and the budding vesicle is finally released into the cytoplasm via a dynamin-mediated membrane fission reaction (Faelber et al., 2012; Ferguson and De Camilli, 2012; Schmid and Frolov, 2011). Previous genetic investigations in many model organisms, including studies of temperature-sensitive alleles in worms and flies (Clark et al., 1997; Koenig and Ikeda, 1989; van der Bliek and Meyerowitz, 1991), as well as knockout and conditional knockout studies in mammalian cells and mice (Ferguson et al., 2007; Ferguson et al., 2009; Liu et al., 2008; Raimondi et al., 2011), strongly supported a critical role of dynamin in endocytic

membrane fission. Such a role is additionally supported by quantitative live-cell imaging, which revealed that the peak of dynamin accumulation at clathrin-coated pits coincides with the membrane fission reaction (Taylor et al., 2012). Likewise, the ability of dynamin to cause fission of membrane tubules has been well established *in vitro* (Bashkirov et al., 2008; Morlot et al., 2012; Pucadyil and Schmid, 2008; Roux et al., 2006). Dynamin assembles into polymers on membrane tubules (Pucadyil and Schmid, 2008; Roux et al., 2006; Zhang and Hinshaw, 2001) and recent structural studies (Chappie et al., 2010; Faelber et al., 2011; Ford et al., 2011) have made progress towards unraveling the detailed molecular mechanism through which dynamin oligomerization and GTP hydrolysis may be coordinated to induce membrane scission.

Mammalian genomes contain three dynamin genes (*DNM1*, *DNM2* and *DNM3*) whose protein products, dynamin 1, 2 and 3, share ~80% overall homology and play at least partially redundant roles during the membrane fission reaction of clathrin-mediated endocytosis (Cao et al., 1998; Cook et al., 1996; Ferguson et al., 2007; Raimondi et al., 2011). However, their expression patterns are very different. Dynamin 1 is expressed selectively and at very high levels in neurons, where it is crucially required for synapses to efficiently recycle synaptic vesicles during intense activity (Ferguson et al., 2007; Hayashi et al., 2008; Lou et al., 2008; Armbruster et al., 2013). Indeed, synaptic transmission defects limit the average lifespan of

dynamain 1 KO mice to less than 2 weeks (Ferguson et al., 2007). Dynamain 2 is expressed ubiquitously (Cao et al., 1998; Cook et al., 1996), and the knockout of dynamain 2 in mice results in early embryonic lethality in agreement with its house-keeping functions (Ferguson et al., 2009). Dynamain 3 is found most prominently in the brain (but at much lower levels than dynamain 1) and testis (Cao et al., 1998; Cook et al., 1996; Ferguson et al., 2007). Although dynamain 3 KO mice do not exhibit obvious neurological or male fertility defects (Raimondi et al., 2011), dynamain 1, 3 double KO mice are more severely affected than dynamain 1 single KOs as revealed by their short lifespan (only several hours), synaptic transmission dysfunction and membrane trafficking defects at synapses (Lou et al., 2012; Raimondi et al., 2011). The additive effect of dynamain 1 and 3 knockout alleles highlights a redundant role of different dynamain isoforms in supporting endocytosis. Endocytosis appears to be controlled, at least to some extent, by the overall abundance of each isoform rather than by major functional differences between them.

Dynamain 2 KO fibroblasts have been used to investigate the contributions of dynamain isoforms to cellular processes common to all cell types (Ferguson et al., 2009; Liu et al., 2008). These cells exhibit defects in clathrin-mediated endocytosis, but such defects are partially compensated by the unexpected expression of dynamain 1 in these cells. Thus, dynamain 1 and 2 double KO mouse fibroblasts (henceforth described as DKO) were generated from mice with floxed dynamain alleles and transgenic for 4-hydroxytamoxifen (OHT)-inducible Cre recombinase (Cre-ER) (Ferguson et al., 2009). Conditional DKO cells can be grown *in vitro* and gene recombination to produce DKO cells can be induced by addition of 4-hydroxytamoxifen. DKO fibroblasts have a much more severe defect in clathrin-mediated endocytosis than cells lacking dynamain 2 alone, although fluid-phase endocytosis is not impaired (Ferguson et al., 2009). Endocytic intermediates that accumulate in these cells are deeply invaginated clathrin-coated pits connected to the plasma membrane by long, narrow tubules. Such tubules are surrounded by BAR-domain-containing proteins, F-actin and actin regulatory proteins (Ferguson et al., 2009). Although DKO cells survived for at least several weeks in culture, they failed to proliferate (Ferguson et al., 2009) and exhibited multiple signaling defects (Shen et al., 2011; Sousa et al., 2012). Given the potential overlapping role of the three dynamain isoforms, we considered the possibility that residual dynamain activity provided by dynamain 3 could support the viability of DKO cells, even if this protein is undetectable by available antibodies in these cells. A definitive assessment of the cellular function of dynamain requires the deletion of all 3 dynamain isoforms. Dynamain triple KO cells would also represent the optimal model to test the dynamain dependence of biological processes and to assess potential off-target action of dynamain inhibitors.

To address these issues, we generated fibroblasts from mice harboring floxed alleles of all three dynamain genes and also expressing Cre-ER. Triple KO (TKO) cells obtained from these conditional KO cells upon tamoxifen-induced gene recombination had the same phenotype as dynamain 1 and 2 DKO cells. Surprisingly, dynasore (Macia et al., 2006) and Dyngo-4a (Harper et al., 2011; Howes et al., 2010; McCluskey et al., 2013), two widely used and structurally related small molecule inhibitors of dynamain, still produced a robust impairment of fluid-phase endocytosis and peripheral membrane ruffles in TKO cells. Given the property of these drugs to cause these very strong effects even in cells where dynamain is absent, caution is required in the interpretation of their cellular action.

## Results

### Generation of dynamain 1, 2 and 3 triple knockout mouse embryonic fibroblasts

In our previous characterization of DKO fibroblasts, we found that these cells remain viable over several weeks in culture but exhibit a severe defect in proliferation (Ferguson et al., 2009). Although immunoblotting experiments with an anti-dynamain-3 antibody that yielded a very strong signal on blot of brain lysates (Ferguson et al., 2007; Raimondi et al., 2011) did not indicate the presence of dynamain 3 in either WT or DKO mouse fibroblasts (Fig. 1A and supplementary material Fig. S1), it remained possible that levels of this dynamain isoform (below our threshold for detection) contributed to the survival of DKO cells. To assess for the potential expression of low levels of the DNM3 gene in mouse fibroblasts, lysates from wild-type cells were affinity purified with immobilized GST fused to SH3 domains 1–4 of Tuba, a high-avidity ligand for all three dynamain isoforms (Ferguson et al., 2007; Salazar et al., 2003), and the bound material was analyzed by mass spectrometry. This strategy detected four peptides that uniquely correspond to the mouse dynamain 3 sequence: K.DFINSELLAQ-LYSSDQNTLMEEAEQAQR.R; K.HVFALFNTEQR.N; R.IE-GSGDQVDTLELSGGAK.I; and R.FLELACDSQEDVDSWK.A, thus demonstrating at least low level expression of this protein in our fibroblast cultures.

To directly determine whether the very low levels of dynamain 3 may perform functions that are essential for viability in DKO cells, we capitalized on the dynamain 1 and 2 conditional double KO (Ferguson et al., 2009) and the dynamain 3 conditional KO (Raimondi et al., 2011) mouse lines that we have previously described. These mutant mice were interbred with one another and with mice transgenic for Cre-ER (Badea et al., 2003; Feil et al., 1996) to generate tamoxifen-inducible triple conditional KO mice (*Dnm1<sup>loxP/loxP</sup>; Dnm2<sup>loxP/loxP</sup>; Dnm3<sup>loxP/loxP</sup>; Cre-ER<sup>+/0</sup>*). These mice were healthy with no obvious abnormalities or fertility defects. Dynamain 1, 2 and 3 TKO cells were generated *in vitro* by tamoxifen treatment of fibroblasts isolated from these mice.

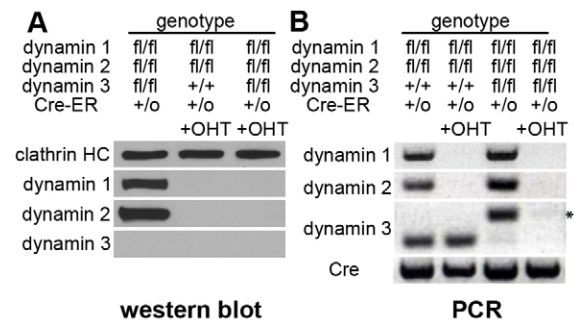


**Fig. 1. Generation of dynamain 1, 2 and 3 TKO fibroblasts.**

(A) Immunoblotting with isoform-specific anti-dynamain antibodies of total homogenates of fibroblasts generated from mice with floxed (fl) dynamain alleles as indicated, and also heterozygous for the transgenic expression of Cre-ER. The anti-clathrin heavy chain (clathrin HC) blot is included as a loading control. +OHT indicates lysates derived from cells treated with 4-hydroxytamoxifen to induce Cre-dependent gene recombination. (B) PCR bands demonstrating recombination of dynamain loci and presence of the Cre recombinase gene. The asterisk indicates a PCR fragment of the floxed allele of dynamain 3, which is larger than the WT allele because of the presence of a loxP site.

Immunoblotting with isoform-specific antibodies did not detect any dynamin signal in these cells (Fig. 1A).

TKO cells ceased to proliferate around day 4 after exposure to tamoxifen, and PCR genotyping of their genomic DNA confirmed the efficient recombination of all three dynamin genes (Fig. 1B). They could re-attach to the substrate and spread following trypsinization (see supplementary material Fig. S3), and their morphology was not grossly different from cells with floxed alleles but untreated with tamoxifen. Thus, the very low expression of dynamin 3 in cultured mouse fibroblast is not essential for the surprising viability of DKO cells, leading to the conclusion that although the function of dynamin is crucial for normal proliferation, dynamin-dependent cellular processes are dispensable for cell viability.

The same results were obtained using another line of dynamin TKO cells that were derived from mutant mice with the following genotype: *Dnm1*<sup>-/-</sup>; *Dnm1loxP/loxP*; *Dnm3*<sup>-/-</sup>; *Cre-ER*<sup>+/-</sup>. Fibroblasts derived from *Cre-ER*<sup>+/-</sup> mice with floxed alleles of all three dynamins were used for all subsequent studies. In all experiments, pools of cells not treated with tamoxifen were used as a control.

### TKO cells display the same endocytic defects observed in DKO cells

As reported for DKO cells (Ferguson et al., 2009), uptake of fluorescent transferrin, a standard assay of clathrin-mediated endocytosis, was drastically impaired in dynamin TKO

fibroblasts (Fig. 2A). In contrast, no inhibition (in fact a slight increase) in the uptake of dextran, a marker of fluid-phase endocytosis, was observed in TKO cells (see Fig. 4).

As expected, in TKO cells, the block in clathrin-dependent internalization of transferrin correlated with an increase in signal for endocytic clathrin coats, as revealed by anti-AP2 ( $\alpha$ -adaptin) immunofluorescence (Fig. 2B). Furthermore, clathrin-coated pits had the typical properties and appearance of the deeply invaginated pits arrested at the pre-fission stage that had been described in DKO cells (Ferguson et al., 2009). First, they had long narrow tubular connections to the plasma membrane, as demonstrated by standard transmission electron microscopy (Fig. 3A–D) and by a positive signal for a cytochemical reaction that selectively labels invaginations connected to the cell surface (Fig. 3E–G). Second, they were enriched in endophilin 2, a BAR-domain-containing protein involved in growth and stabilization of the tubular membrane neck of clathrin-coated pits (Fig. 2C) and for the Arp2/3 (p34 subunit) actin nucleating complex (Fig. 2D) (Ferguson et al., 2009).

Other changes observed in DKO cells relative to controls, such as a major reduction of caveolin levels (Ferguson et al., 2009) and a robust increase in acetylated tubulin (Ferguson et al., 2009; Tanabe and Takei, 2009) were observed in TKO cells (supplementary material Fig. S2). These effects were not investigated further and it remains unknown whether or not they reflect direct actions of dynamin in these processes.

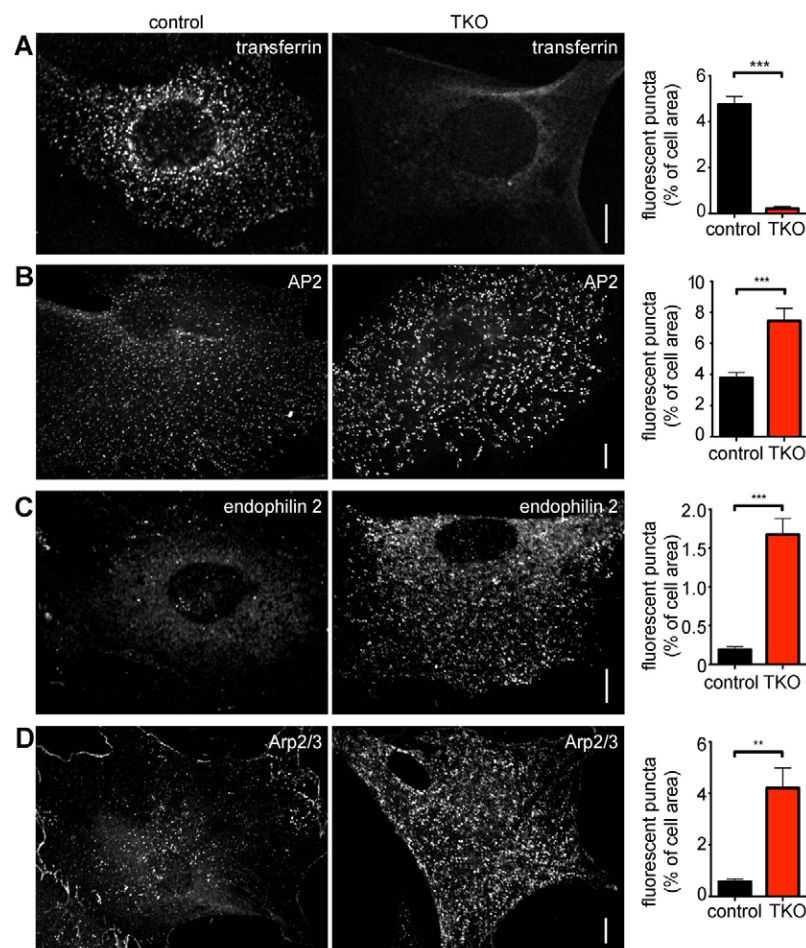


**Fig. 2. Defects in clathrin-mediated endocytosis and actin distribution in dynamin TKO cells.** (A) Impaired internalization of fluorescent transferrin in TKO cells. (B) Increased abundance of endocytic clathrin-coated pits in TKO cells as revealed by immunofluorescence for the  $\alpha$ -adaptin subunit of the AP2 clathrin adaptor complex. (C,D) Increased abundance in TKO cells of endophilin 2 (C)- and Arp 2/3 (ARPC2 subunit; D)-positive puncta. These puncta are known to reflect the accumulation of these proteins at the collars of arrested clathrin-coated pits in dynamin-deficient cells (Ferguson et al., 2009). Quantifications of the fluorescence signals for all conditions are shown on the right (5–18 cells per condition). Scale bars: 10  $\mu$ m.

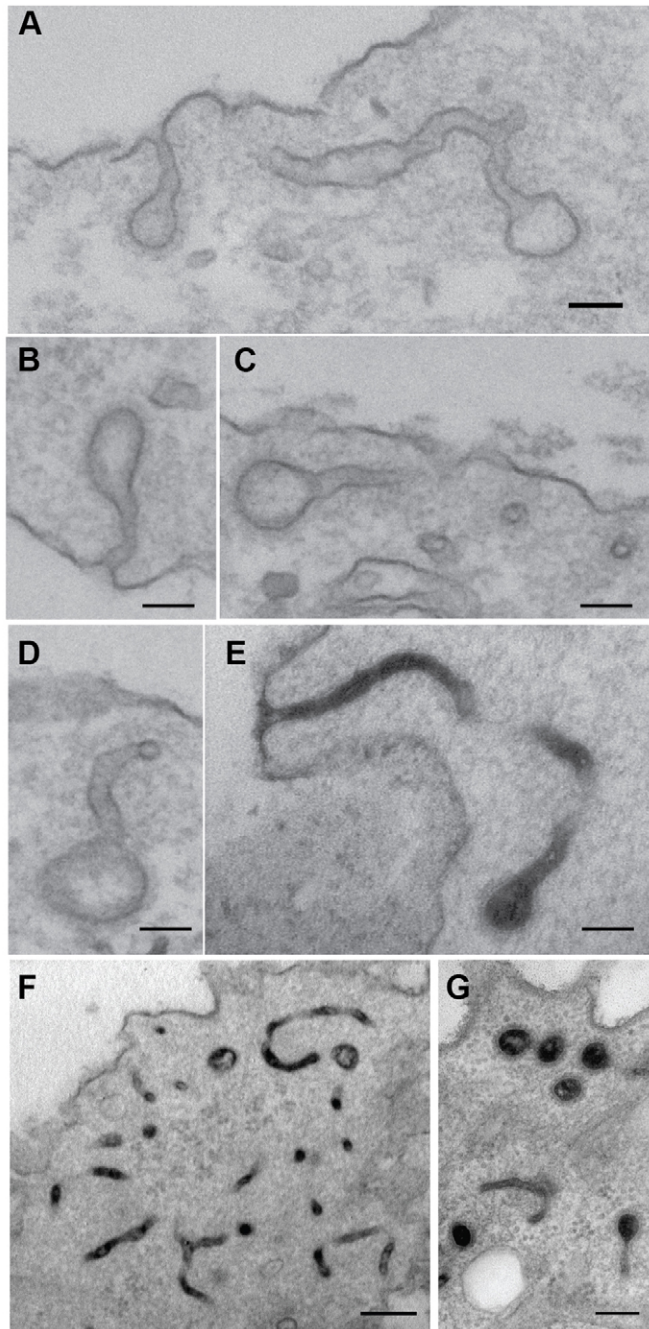


**Fig. 3. Clathrin-coated pits connected to the plasma membrane by long, narrow tubular necks in dynamin TKO cells.** (A–D) Representative EM images from conventionally stained sections. (E–G) Presence of electron dense material in tubular invaginations of the plasma membrane, some of which are capped by a clathrin-coated bud in the plane of the section, following a cytochemical reaction (black reaction product) that selectively labels internal structures continuous with plasma membrane. Scale bars: 100 nm (A–E), 400 nm (F); 200 nm (G).

In summary, the similar viability and endocytic phenotypes observed in DKO and in TKO cells do not support a major relevant contribution of the very low levels of dynamin 3 to these features in fibroblasts.

### TKO cells unmask dynamin-independent effects of dynasore and Dyngo-4a

TKO cells provide the opportunity to investigate the specificity of dynamin inhibitors. We focused on two commonly used dynamin inhibitors, dynasore and Dyngo-4a. Dynasore, the first reported dynamin inhibitor (Macia et al., 2006), is widely used to investigate the role of dynamin in cellular events. Dyngo-4a, a close structural analog of dynasore, has been increasingly used in recent studies because of its higher potency in dynamin inhibition (Harper et al., 2011; Howes et al., 2010; McCluskey et al., 2013). We reasoned that if the effects of these dynamin inhibitors on cells are mediated through dynamin binding and inhibition, then cells that lack dynamin (i.e. TKO cells) should be insensitive to these drugs.

As mentioned above, fluid-phase endocytosis is not impaired in TKO cells relative to the control cells. Dynasore has been reported to inhibit this endocytic pathway (Macia et al., 2006) and we confirmed this effect in WT cells, and found that Dyngo-4a inhibits this pathway to a similar degree and does so at a lower concentration (Harper et al., 2011; Howes et al., 2010; McCluskey et al., 2013). Surprisingly, both dynasore and Dyngo-4a were still able to inhibit dextran uptake even in the TKO cells (Fig. 4A,B).

Although dynamin TKO cells did not exhibit obvious defects, relative to controls, in morphology or in attachment and spreading after replating, dynasore was shown to inhibit cell spreading (Macia et al., 2006) and to suppress the formation of lamellipodia (Yamada et al., 2009). We have now observed that dynasore triggers these effects even in TKO cells, as staining of F-actin with phalloidin revealed the shrinkage of TKO cells after dynasore treatment (supplementary material Fig. S3).

To further investigate the effect of dynasore and Dyngo-4a on the actin cytoskeleton, TKO cells transiently expressing a fluorescent F-actin reporter (the calponin homology domain of utrophin fused to GFP) (Burkel et al., 2007) were imaged by time-lapse spinning disk confocal microscopy before and during treatment with dynasore or Dyngo-4a. Inspection of cortical cell regions showed membrane ruffles that extended and retracted over a distance of several micrometers over a period of a few seconds in both control or TKO fibroblasts, revealing the dynamin independence of this process (supplementary material Fig. S4). However, the intense F-actin signal in lamellipodia was lost in both control and TKO cells following either dynasore or Dyngo-4a treatment (Fig. 5A,B; supplementary material Movies 2, 3, 5, 6, 8, 9, 11, 12), whereas no effect was observed after addition of DMSO, the solvent used to solubilize dynasore and Dyngo-4a (supplementary material Fig. S4 and Movies 1, 4, 7, 10.). The drastic inhibition (Fig. 5D) occurred within minutes of drug addition, as shown by galleries of time-lapse images (Fig. 5C) and quantitative data of membrane ruffling (Fig. 5E). We conclude that dynamin does not play an essential role in peripheral membrane ruffling and that the cessation of membrane ruffling in TKO cells upon dynasore or Dyngo-4a treatment arises from an off-target effect of these inhibitors.

### Discussion

In this study, we have reported the generation and characterization of dynamin 1, 2 and 3 triple conditional KO mouse fibroblasts. Following Cre-recombinase-induced inactivation of all three genes, these cells lose expression of all three dynamins. TKO cells display the major defects previously observed in DKO cells, without additional obvious changes,

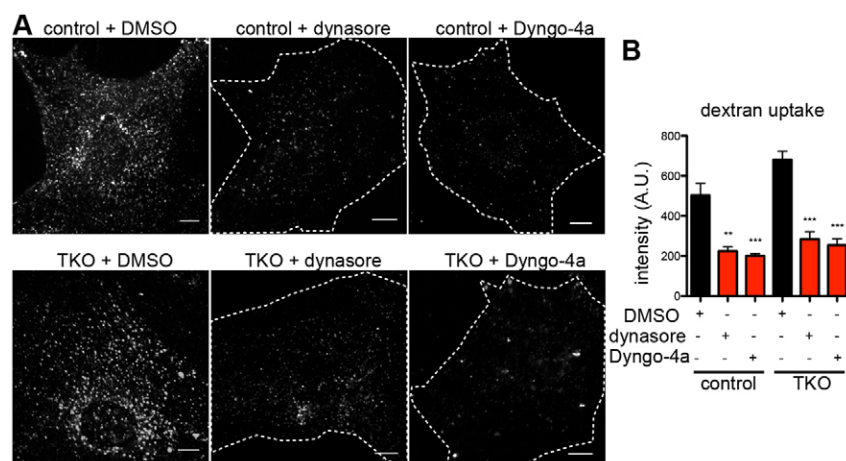


**Fig. 4. Fluid-phase endocytosis is not impaired in TKO cells, but is inhibited by dynasore or Dyngo-4a in both control and TKO cells.** (A) Fluorescence images showing that Alexa-Fluor-488-dextran internalization is not impaired (in fact slightly enhanced) in TKO cells relative to control cells, but is strongly inhibited by dynasore or Dyngo-4a. The periphery of dynasore- and Dyngo-4a-treated cells is outlined by dotted lines. Scale bars: 10  $\mu$ m. (B) Quantification of the results shown in A;  $n=10$  cells per condition. DMSO, which was used to dissolve dynasore or Dyngo-4a, was present in control and drug-treated cells at the final concentration of 0.15% (+DMSO), 0.15% (+dynasore), and 0.1% (+Dyngo-4a).

supporting conclusions on the overall cellular functions of dynamin reported in studies of DKO cells (Ferguson et al., 2009). Thus, although we have now found that very low levels of dynamin 3 can be detected in mouse fibroblasts in culture, as detected by affinity purification and mass spectrometry, this small pool of dynamin 3 does not contribute significantly to

fibroblast physiology. This result contrasts with observations in neurons where the absence of the major neuronal dynamin, dynamin 1, unmasks an important function of dynamin 3 in synaptic physiology, as dynamin 1 and 3 double knockout neurons exhibit more severe defects in synaptic function than dynamin 1 KO neurons (Lou et al., 2012; Raimondi et al., 2011).

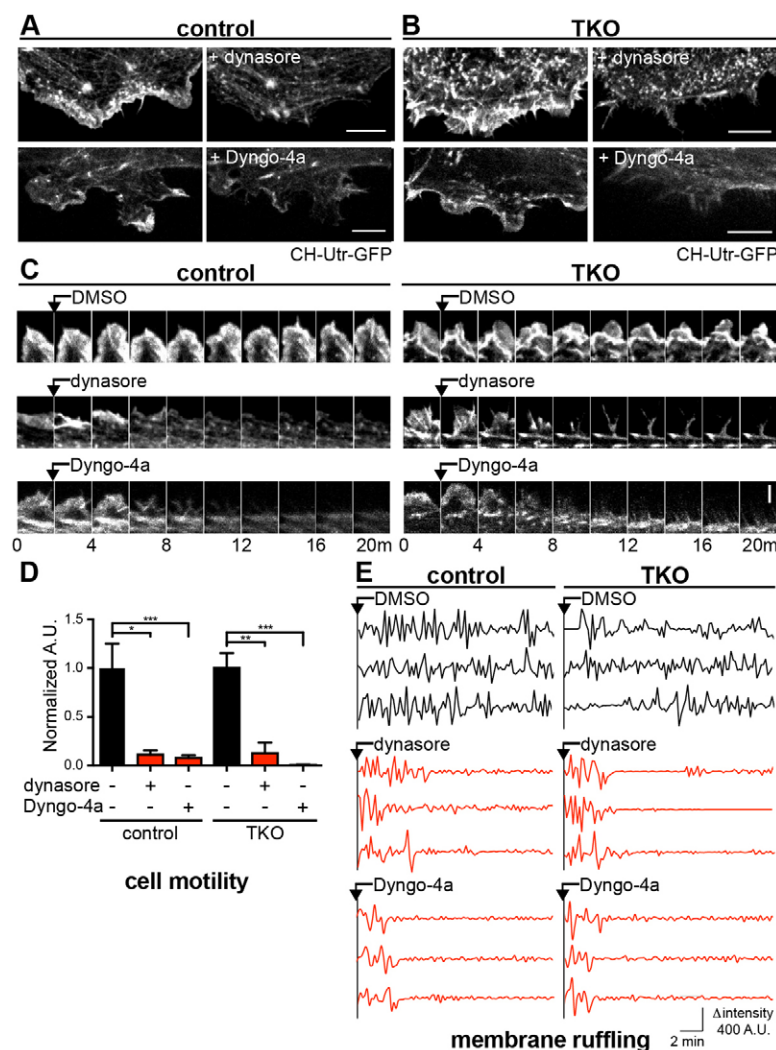


**Fig. 5. Dynasore and Dyngo-4a inhibit peripheral membrane ruffling in both control and TKO cells.** Analysis of the effect of dynasore (80  $\mu$ M, 37°C) or Dyngo-4a (30  $\mu$ M, 37°C) on peripheral membrane ruffling in control and TKO cells expressing calponin homology (CH) domain of utrophin (CH-Utr, a live marker of F-actin) fused to GFP (spinning disk confocal microscopy). Fluorescence images of small regions of the cell periphery of control (A) and TKO cells (B) expressing CH-Utr fused to GFP before and after 20 minutes incubation with dynasore (top) or Dyngo-4a (bottom), showing the disrupting effect of these drugs on the ruffles in both control and TKO cells. (C) Time series (120 second intervals) of cropped images of the edge of control (left) and TKO (right) cells showing persistence of membrane ruffles over 20 minutes (top), but their rapid disappearance in response to dynasore (middle) or Dyngo-4a (bottom), but not in response to the DMSO used to solubilize these drugs (top). (D) Quantification of cell motility of control and TKO cells in response to dynasore or Dyngo-4a;  $n=3-5$  cells per condition. (E) Representative graphs showing the fluorescence intensity changes of three randomly selected points in membrane ruffles of control (left) or TKO (right) cells in the absence and presence of dynasore or Dyngo-4a. Scale bars: 10  $\mu$ m (A,B); 3  $\mu$ m (C). DMSO, which was used to dissolve dynasore, was present in control and dynasore-treated cells at the final concentration of 0.15% (DMSO only), 0.15% (dynasore treatment) or 0.1% (Dyngo-4a treatment).

Our results corroborate our hypothesis that a primary function of dynamin is to support clathrin-mediated endocytosis (Ferguson et al., 2009; Ferguson and De Camilli, 2012), as fluid-phase endocytosis appeared to be unperturbed in TKO fibroblasts. Similar results were observed in dynamin 1 KO neurons and also in dynamin 1 and 3 DKO neurons (i.e. nerve terminals nearly devoid of dynamin). In these neurons, clathrin-mediated endocytosis of synaptic vesicles was strongly impaired, while robust bulk endocytosis, a form of fluid-phase endocytosis, persisted [(Hayashi et al., 2008) and our unpublished observations]. Partial impairment of dynamin function by non-pharmacological methods was shown to inhibit fluid-phase endocytosis in some studies (Cao et al., 2007; Damke et al., 1995), but not in others (Liu et al., 2008; Schlunck et al., 2004). The disruption of all three dynamin genes, as we have done here, provides an unambiguous system to test the cellular processes that do and do not require this extensively studied GTPase.

The generation of dynamin TKO cells allowed us to study the specificity of the effects of two structurally related, widely used dynamin inhibitors, dynasore and Dyngo-4a. Dynasore was shown to inhibit not only clathrin-mediated endocytosis, but also fluid-phase endocytosis (Macia et al., 2006), a finding that we have confirmed. As we have demonstrated here, Dyngo-4a also inhibits this endocytic pathway. However, we have observed that both dynasore and Dyngo-4a still produce the inhibitory effect on fluid-phase endocytosis in cells where its intended target, dynamin, has been eliminated, indicating that this action represents an off-target effect. Additionally, we have found that both dynasore and Dyngo-4a have a powerful blocking effect on membrane ruffling and that this action is also independent of dynamin as it still occurs in TKO cells. This result does not exclude the possibility that dynamin may have some regulatory role in ruffle dynamics given its localization in ruffles and its many interactions with actin regulatory proteins (McNiven et al., 2000; Orth and McNiven, 2003; Schafer, 2004; Yamada et al., 2013), but strongly cautions against the use of these dynamin inhibitors as tools to investigate the role of dynamin in this process.

The mechanisms whereby dynasore, a noncompetitive inhibitor of the GTPase activity of dynamin (Macia et al., 2006), and its close structural analog Dyngo-4a (Harper et al., 2011; Howes et al., 2010; McCluskey et al., 2013) produce their off-target effects remain unknown. Dynasore was originally shown to also inhibit Drp1, a dynamin-like GTPase involved in mitochondrial division, although less efficiently (Macia et al., 2006). Effects of this drug on other members (Faelber et al., 2013; Ferguson and De Camilli, 2012) of the dynamin superfamily of GTPases are a possibility. However, off-target effects of dynasore and Dyngo-4a may also be due to GTPase-independent actions. In addition to dynasore and Dyngo-4a, a variety of other dynamin inhibitors have recently been developed, including Iminodyn-22 (Hill et al., 2010), Dynole 34-2 (Hill et al., 2009), RTIL-13 (Zhang et al., 2008), MiTMAB and OcTMAB (Quan et al., 2007), and indole 24 and 25 (Gordon et al., 2013). Given the findings reported here concerning the non-specific effects on dynasore and Dyngo-4a on fluid-phase endocytosis and membrane ruffling, results arising from the use of such chemicals should be interpreted with caution and be corroborated by independent methods. For example, inhibition of VEGFR2 signaling in endothelial cells by dynasore was taken as an indication that signaling by this receptor is dependent on

endocytosis (Sawamiphak et al., 2010; Wang et al., 2010). However, the opposite result, increased signaling of VEGFR2, was observed in endothelial cells where internalization of VEGFR2 was inhibited by the genetic ablation of the endocytic adaptors epsin 1 and 2 (Pasula et al., 2012), or by RNAi-mediated suppression of dynamin 2 (Satish Pasula, Hong Chen, William Sessa and P. D. C., unpublished observations). Genetic models, such as the dynamin TKO cells presented in this study, should serve as an important tool in the conclusive assessment of the dynamin dependence of results obtained with dynamin inhibitors.

Abnormal dynamin function has been linked to diseases in humans and animals. Mutations in the ubiquitously expressed dynamin 2 isoform cause specific, dominantly inherited forms of Charcot-Marie-Tooth disease and centronuclear myopathy in humans (Bitoun et al., 2005; Züchner et al., 2005). Based on disorders arising from dynamin mutations in other mammals, such as exercise-induced collapse in dogs (Patterson et al., 2008) and seizures in the *fitful* mouse (Boumil et al., 2010), additional dynamin-dependent conditions probably remain undiscovered in humans. Dynamin TKO cells represent a powerful system for testing the function of disease-related mutations of dynamin.

## Materials and Methods

### Generation of dynamin 1, 2 and 3 conditional triple knockout mouse fibroblasts and cell cultures

The conditional KO (floxed) and KO alleles of dynamin 1, 2 and 3 used in this study were previously described (Ferguson et al., 2007; Ferguson et al., 2009; Raimondi et al., 2011). Animal care and use were in accordance with our institutional guidelines.

Fibroblast cultures were derived from mice and maintained as previously described (Ferguson et al., 2009). The homologous recombination of the conditional KO alleles was carried out by the activation of an estrogen-receptor-Cre-recombinase fusion protein (Cre-ER) upon 4-hydroxytamoxifen (Sigma) treatment according to our previously established protocol (Ferguson et al., 2009). Briefly, cells were incubated with 3  $\mu$ M tamoxifen for 2 days, resulting in dynamin depletion at 5–6 days from the start of the treatment period. TKO cells were generally used for experiments between 7 and 9 days. Control cells were the triple conditional KO cells without 4-hydroxytamoxifen treatment. Cell culture, immunoblotting and immunofluorescence were performed as described previously (Ferguson et al., 2009).

Cells for imaging experiments were electroporated with the Amaxa Nucleofector method (protocol A-24) and grown for 16–24 hours in culture medium on 12 mm glass coverslips or on 35 mm glass bottom dishes (Mat-Tek, Ashland, MA, USA) at sub-confluent densities.

### PCR of genomic DNA

DNeasy Blood and Tissue Kit (Qiagen) was used to extract genomic DNA from cultured fibroblasts. The following oligonucleotide primers were used for PCR-based genotyping of the respective alleles: floxed allele of dynamin 1: 5'-TTG-TGTATGTGAGTGCACCCATGC-3' and 5'-CAGCTGGGTATAATGAGGCCT-CATC-3'; floxed allele of dynamin 2: 5'-GCAGGAAGACACAACTGAAC-3' and 5'-CCTGCTAGTGACCTTTCTTGAG-3'; floxed allele of dynamin 3: 5'-GACATGTTAAACATAGGCTAAACC-3' and 5'-CAGTGCTTCCAAGTTCATT-CC-3'; Esr-Cre transgene: 5'-CTTGCATGATCCGGTATTGA-3' and 5'-ACATTGGGCGCTAAACATG-3'.

### Antibodies and plasmids

The following antibodies were obtained from commercial sources: mouse anti-clathrin heavy chain (clone TD1, Affinity Bioreagents), mouse anti- $\alpha$ -adaptin (AP2 subunit; clone AP6, Affinity Bioreagents), rabbit anti-dynamin 1 (Epitomics, Burlingame, CA), mouse anti-acetylated  $\alpha$ -tubulin (Sigma), mouse anti-caveolin 1 (BD Biosciences, San Jose, CA), rabbit anti-ARPC2 (Arp2/3) (Millipore, Billerica, MA), rabbit anti-GAPDH (Abcam, ab9485). Anti-rabbit and anti-mouse IgG (H<sup>+</sup>L) HRP-conjugated secondary antibodies were obtained from BioRad (Hercules, CA). Alexa-Fluor-594-phalloidin and Alexa-Fluor-488- or -594-conjugated secondary antibodies were obtained from Invitrogen. The following antibodies were previously generated in our laboratory: rabbit anti-endophilin 2 (Milosevic et al., 2011), rabbit anti-dynamin 2 and mouse anti-dynamin 3 (Ferguson et al., 2007). A plasmid expressing the GFP-tagged calponin homology domain of utrophin (Utr-CH) was kindly provided by William Bement (University of Wisconsin–Madison) (Burkel et al., 2007).

## Imaging

For epifluorescence imaging, samples were imaged with a Zeiss Axioplan2 microscope using a Plan-Apochromatic 40 $\times$  objective and a Hamamatsu ORCA II digital camera under the control of MetaMorph v7.1.2 software (Molecular Devices). For confocal imaging, cells were imaged on a Zeiss LSM 710 laser scanning confocal microscope equipped with a 63 $\times$  objective using ZEN (Carl Zeiss, Inc.) software or by spinning disk confocal microscopy: Improvision UltraVIEW VoX system including a Nikon Ti-E Eclipse inverted microscope (equipped with a 603 CFI PlanApo VC, NA 1.4 objective) and a spinning disk confocal scan head (CSU-X1, Yokogawa) driven by Velocity (Improvision) software.

For fixed samples, a 2  $\mu$ m thick section was imaged with optical sections acquired at 100 nm intervals in the z-axis with exposure times that ranged from 150 msec to 300 msec. The slices were iteratively deconvolved with Velocity software, and collapsed to a single image by maximal intensity projection with ImageJ software (version 1.43u, NIH). For living cells, imaging was performed at 37°C on a heated stage in Phenol-Red-free Dulbecco's Modified Eagle's Medium (DMEM) supplemented with high glucose and L-glutamine (Gibco). Time-lapse images were taken at a rate of 5 frames per minute and exposure times ranged from 50 to 100 msec per frame.

## Electron microscopy

Dynamins TKO cells were grown overnight on 35 mm glass bottomed (thickness=0.15 mm) dishes (Mat-Tek), washed with PBS and then fixed in 2.5% glutaraldehyde in 0.1 M sodium cacodylate buffer (pH 7.4) for 1 hour at room temperature. Following washing with 0.1 M sodium cacodylate buffer, cells were post-fixed in 1% OsO<sub>4</sub> in 0.1 M cacodylate buffer for 1 hour at room temperature, washed in 50 mM sodium maleate buffer (pH 5.2), and *en bloc* stained with 2% uranyl acetate in 50 mM sodium maleate buffer (pH 5.2) for 1 hour in the dark. Cells were then dehydrated and embedded as previously described (Ferguson et al., 2007).

For the cytochemical labeling of surface-exposed membrane, glutaraldehyde-fixed cells were rinsed, incubated in 0.25% OsO<sub>4</sub> + 0.25% potassium ferrocyanide solution for 15 minutes, rinsed three times with cacodylate buffer, incubated for 15 minutes in 1% tannic acid, washed with cacodylate buffer (three times, 5 minutes each) and then with acetate buffer (three times, 5 minutes each) and finally stained *en bloc* with uranyl acetate as described above. All the solutions were made up in cacodylate buffer except for the uranyl acetate solution. The rapid washes allow some remaining tannic acid to react with uranyl salts to form a colloid, resulting in electron-dense staining on the plasma membrane and its invaginations in particular. This method was developed and communicated to us by John Heuser (Washington University and Kyoto University).

## Endocytic assays

For dextran uptake, cells were incubated for 30 minutes at 37°C in the presence of fixable Alexa-Fluor-488-conjugated dextran (10,000 MW; Invitrogen) at a concentration of 0.5 mg/ml in Phenol-Red-free DMEM. For transferrin uptake, 5  $\mu$ g/ml Alexa-Fluor-488-transferrin was bound to cells for 30 minutes at 4°C and further incubated at 4°C for 10 minutes. Cells were washed in PBS, fixed, mounted and visualized by confocal microscopy.

## Dynasore treatment

Dynasore with >99% purity (Tocris) and Dyngo-4a (Abcam) were dissolved in DMSO to make stock solutions, aliquoted and stored at -20°C (Kirchhausen et al., 2008). For immunofluorescence, cells were rinsed twice in DMEM, incubated with dynasore (80  $\mu$ M) or Dyngo-4a (30  $\mu$ M) in DMEM at 37°C for 30 minutes, then fixed and further processed as described above. For live-cell imaging, cells were washed twice in imaging buffer (Phenol-Red-free DMEM), and dynasore (80  $\mu$ M final) or Dyngo-4a (30  $\mu$ M) was added to the dish during image acquisition. For control experiments, an equivalent concentration of DMSO (~0.15%) was added.

## Image analysis and statistics

Fluorescent spots in fixed control and TKO cells were analyzed using ImageJ after background subtraction. For the quantification of fluorescent transferrin and of immunoreactivity for AP2, endophilin 2 and Arp2/3, all fluorescent puncta in a cell were selected and normalized against the footprint of the cell. For the quantification of dextran uptake, the fluorescent intensity of dextran in a cell ( $n=10$  cells) was measured and normalized against the cell footprint. For cell motility measurement in living cells, images were acquired at 12 second interval for 20 minutes by spinning disk confocal microscopy. Image time series were registered using the StackReg plug-in of ImageJ (Biomedical Imaging Group, École Polytechnique Fédérale de Lausanne, Switzerland). For the quantification of cell motility (Fig. 5D), images of each time point were subtracted from the image taken 48 seconds later. The resultant set of subtracted images was z-projected onto a single image using an average intensity method (ImageJ) and the change in fluorescent signal at the cell edge was quantified and normalized to the length of the cell perimeter. For the analysis of membrane ruffling (Fig. 5E), the change in

fluorescence intensity of three randomly selected regions of interest (2 $\times$ 2 pixels) at the cell periphery in control or TKO cells upon DMSO, dynasore or Dyngo-4a treatment was measured. All data except those of membrane ruffling are presented as means  $\pm$  s.e.m. (GraphPad Prism Software, La Jolla California USA). Statistical significance was determined using Student's *t*-tests; \*\*\**P*<0.001, \*\**P*<0.01 and \**P*<0.02.

## Acknowledgements

We thank Frank Wilson, Louise Lucast and Stacy Wilson for outstanding lab support, John Heuser for the communication of unpublished methods, Olof Idevall-Hagren, Mirko Messa and Jeremy Baskin for discussions.

## Author contributions

R.J.P., H.S., S.M.F. and P.D.C. designed research; R.J.P., H.S., S.M.F., X.L., and L.L. conducted experiments; R.J.P. and H.S. analyzed data; and R.J.P., H.S., S.M.F. and P.D.C. wrote the paper.

## Funding

This work was supported by grants from the National Institutes of Health [grant numbers R37NS036251, P30DK045735 and P30DA018343 to P.D.C.] and from the Ellison Medical Foundation to P.D.C. and S.M.F. Deposited in PMC for release after 12 months.

Supplementary material available online at

<http://jcs.biologists.org/lookup/suppl/doi:10.1242/jcs.138578/-/DC1>

## Reference

- Armbruster, M., Messa, M., Ferguson, S. M., De Camilli, P. and Ryan, T. A. (2013). Dynamins phosphorylation controls optimization of endocytosis for brief action potential bursts. *eLife* **2**, e00845.
- Badea, T. C., Wang, Y. and Nathans, J. (2003). A noninvasive genetic/pharmacologic strategy for visualizing cell morphology and clonal relationships in the mouse. *J. Neurosci.* **23**, 2314-2322.
- Bashkurov, P. V., Akimov, S. A., Evseev, A. I., Schmid, S. L., Zimmerberg, J. and Frolov, V. A. (2008). GTPase cycle of dynamins is coupled to membrane squeeze and release, leading to spontaneous fission. *Cell* **135**, 1276-1286.
- Bitoun, M., Maugendre, S., Jeannot, P. Y., Lacène, E., Ferrer, X., Laforêt, P., Martin, J. J., Laporte, J., Lochmüller, H., Beggs, A. H. et al. (2005). Mutations in dynamins 2 cause dominant centronuclear myopathy. *Nat. Genet.* **37**, 1207-1209.
- Boumil, R. M., Letts, V. A., Roberts, M. C., Lenz, C., Mahaffey, C. L., Zhang, Z. W., Moser, T. and Frankel, W. N. (2010). A missense mutation in a highly conserved alternate exon of dynamins-1 causes epilepsy in fitful mice. *PLoS Genet.* **6**, e1001046.
- Brodin, L., Löw, P. and Shupliakov, O. (2000). Sequential steps in clathrin-mediated synaptic vesicle endocytosis. *Curr. Opin. Neurobiol.* **10**, 312-320.
- Burkel, B. M., von Dassow, G. and Bement, W. M. (2007). Versatile fluorescent probes for actin filaments based on the actin-binding domain of utrophin. *Cell Motil. Cytoskeleton* **64**, 822-832.
- Cao, H., Garcia, F. and McNiven, M. A. (1998). Differential distribution of dynamins isoforms in mammalian cells. *Mol. Biol. Cell* **9**, 2595-2609.
- Cao, H., Chen, J., Awoniyi, M., Henley, J. R. and McNiven, M. A. (2007). Dynamins 2 mediates fluid-phase micropinocytosis in epithelial cells. *J. Cell Sci.* **120**, 4167-4177.
- Chappie, J. S., Acharya, S., Leonard, M., Schmid, S. L. and Dyda, F. (2010). G domain dimerization controls dynamins assembly-stimulated GTPase activity. *Nature* **465**, 435-440.
- Clark, S. G., Shurland, D. L., Meyerowitz, E. M., Bargmann, C. I. and van der Bliek, A. M. (1997). A dynamins GTPase mutation causes a rapid and reversible temperature-inducible locomotion defect in *C. elegans*. *Proc. Natl. Acad. Sci. USA* **94**, 10438-10443.
- Conner, S. D. and Schmid, S. L. (2003). Regulated portals of entry into the cell. *Nature* **422**, 37-44.
- Cook, T., Mesa, K. and Urrutia, R. (1996). Three dynamins-encoding genes are differentially expressed in developing rat brain. *J. Neurochem.* **67**, 927-931.
- Damke, H., Baba, T., van der Bliek, A. M. and Schmid, S. L. (1995). Clathrin-independent pinocytosis is induced in cells overexpressing a temperature-sensitive mutant of dynamins. *J. Cell Biol.* **131**, 69-80.
- Dittman, J. and Ryan, T. A. (2009). Molecular circuitry of endocytosis at nerve terminals. *Annu. Rev. Cell Dev. Biol.* **25**, 133-160.
- Doherty, G. J. and McMahon, H. T. (2009). Mechanisms of endocytosis. *Annu. Rev. Biochem.* **78**, 857-902.
- Faelber, K., Posor, Y., Gao, S., Held, M., Roske, Y., Schulze, D., Hauke, V., Noé, F. and Daumke, O. (2011). Crystal structure of nucleotide-free dynamins. *Nature* **477**, 556-560.
- Faelber, K., Held, M., Gao, S., Posor, Y., Hauke, V., Noé, F. and Daumke, O. (2012). Structural insights into dynamins-mediated membrane fission. *Structure* **20**, 1621-1628.

- Faelber, K., Gao, S., Held, M., Posor, Y., Hauke, V., Noé, F. and Daumke, O. (2013). Oligomerization of dynamin superfamily proteins in health and disease. *Prog. Mol. Biol. Transl. Sci.* **117**, 411-443.
- Feil, R., Brocard, J., Mascres, B., LeMeur, M., Metzger, D. and Chambon, P. (1996). Ligand-activated site-specific recombination in mice. *Proc. Natl. Acad. Sci. USA* **93**, 10887-10890.
- Ferguson, S. M. and De Camilli, P. (2012). Dynamin, a membrane-remodelling GTPase. *Nat. Rev. Mol. Cell Biol.* **13**, 75-88.
- Ferguson, S. M., Brasnjo, G., Hayashi, M., Wölfel, M., Collesi, C., Giovedi, S., Raimondi, A., Gong, L. W., Ariel, P., Paradise, S. et al. (2007). A selective activity-dependent requirement for dynamin 1 in synaptic vesicle endocytosis. *Science* **316**, 570-574.
- Ferguson, S. M., Raimondi, A., Paradise, S., Shen, H., Mesaki, K., Ferguson, A., Destaing, O., Ko, G., Takasaki, J., Cremona, O. et al. (2009). Coordinated actions of actin and BAR proteins upstream of dynamin at endocytic clathrin-coated pits. *Dev. Cell* **17**, 811-822.
- Ford, M. G., Jenni, S. and Nunnari, J. (2011). The crystal structure of dynamin. *Nature* **477**, 561-566.
- Gordon, C. P., Venn-Brown, B., Robertson, M. J., Young, K. A., Chau, N., Mariana, A., Whiting, A., Chircop, B., Robinson, P. J. and McCluskey, A. (2013). Development of second-generation indole-based dynamin GTPase inhibitors. *J. Med. Chem.* **56**, 46-59.
- Harper, C. B., Martin, S., Nguyen, T. H., Daniels, S. J., Lavidis, N. A., Popoff, M. R., Hadzic, G., Mariana, A., Chau, N., McCluskey, A. et al. (2011). Dynamin inhibition blocks botulinum neurotoxin type A endocytosis in neurons and delays botulism. *J. Biol. Chem.* **286**, 35966-35976.
- Hayashi, M., Raimondi, A., O'Toole, E., Paradise, S., Collesi, C., Cremona, O., Ferguson, S. M. and De Camilli, P. (2008). Cell- and stimulus-dependent heterogeneity of synaptic vesicle endocytic recycling mechanisms revealed by studies of dynamin 1-null neurons. *Proc. Natl. Acad. Sci. USA* **105**, 2175-2180.
- Heuser, J. E. and Reese, T. S. (1973). Evidence for recycling of synaptic vesicle membrane during transmitter release at the frog neuromuscular junction. *J. Cell Biol.* **57**, 315-344.
- Hill, T. A., Gordon, C. P., McGeachie, A. B., Venn-Brown, B., Odell, L. R., Chau, N., Quan, A., Mariana, A., Sakoff, J. A., Chircop, M. et al. (2009). Inhibition of dynamin mediated endocytosis by the dynoles – synthesis and functional activity of a family of indoles. *J. Med. Chem.* **52**, 3762-3773.
- Hill, T. A., Mariana, A., Gordon, C. P., Odell, L. R., Robertson, M. J., McGeachie, A. B., Chau, N., Daniel, J. A., Gorgani, N. N., Robinson, P. J. et al. (2010). Iminochromene inhibitors of dynamins I and II GTPase activity and endocytosis. *J. Med. Chem.* **53**, 4094-4102.
- Howes, M. T., Kirkham, M., Riches, J., Cortese, K., Walser, P. J., Simpson, F., Hill, M. M., Jones, A., Lundmark, R., Lindsay, M. R. et al. (2010). Clathrin-independent carriers form a high capacity endocytic sorting system at the leading edge of migrating cells. *J. Cell Biol.* **190**, 675-691.
- Kirchhausen, T. (2000). Three ways to make a vesicle. *Nat. Rev. Mol. Cell Biol.* **1**, 187-198.
- Kirchhausen, T., Macia, E. and Pelish, H. E. (2008). Use of dynasore, the small molecule inhibitor of dynamin, in the regulation of endocytosis. *Methods Enzymol.* **438**, 77-93.
- Koenig, J. H. and Ikeda, K. (1989). Disappearance and reformation of synaptic vesicle membrane upon transmitter release observed under reversible blockage of membrane retrieval. *J. Neurosci.* **9**, 3844-3860.
- Liu, Y. W., Surka, M. C., Schroeter, T., Lukiyanchuk, V. and Schmid, S. L. (2008). Isoform and splice-variant specific functions of dynamin-2 revealed by analysis of conditional knock-out cells. *Mol. Biol. Cell* **19**, 5347-5359.
- Lou, X., Paradise, S., Ferguson, S. M. and De Camilli, P. (2008). Selective saturation of slow endocytosis at a giant glutamatergic central synapse lacking dynamin 1. *Proc. Natl. Acad. Sci. USA* **105**, 17555-17560.
- Lou, X., Fan, F., Messa, M., Raimondi, A., Wu, Y., Looger, L. L., Ferguson, S. M. and De Camilli, P. (2012). Reduced release probability prevents vesicle depletion and transmission failure at dynamin mutant synapses. *Proc. Natl. Acad. Sci. USA* **109**, E515-E523.
- Macia, E., Ehrlich, M., Massol, R., Boucrot, E., Brunner, C. and Kirchhausen, T. (2006). Dynasore, a cell-permeable inhibitor of dynamin. *Dev. Cell* **10**, 839-850.
- McCluskey, A., Daniel, J. A., Hadzic, G., Chau, N., Clayton, E. L., Mariana, A., Whiting, A., Gorgani, N., Lloyd, J., Quan, A. et al. (2013). Building a Better Dynasore: The Dyngo Compounds Potently Inhibit Dynamin and Endocytosis. *Traffic*. doi: 10.1111/tra.12119. [Epub ahead of print]
- McNiven, M. A., Kim, L., Krueger, E. W., Orth, J. D., Cao, H. and Wong, T. W. (2000). Regulated interactions between dynamin and the actin-binding protein cortactin modulate cell shape. *J. Cell Biol.* **151**, 187-198.
- Milosevic, I., Giovedi, S., Lou, X., Raimondi, A., Collesi, C., Shen, H., Paradise, S., O'Toole, E., Ferguson, S., Cremona, O. et al. (2011). Recruitment of endophilin to clathrin-coated pit necks is required for efficient vesicle uncoating after fission. *Neuron* **72**, 587-601.
- Morlot, S., Galli, V., Klein, M., Chiaruttini, N., Manzi, J., Humbert, F., Dinis, L., Lenz, M., Cappello, G. and Roux, A. (2012). Membrane shape at the edge of the dynamin helix sets location and duration of the fission reaction. *Cell* **151**, 619-629.
- Orth, J. D. and McNiven, M. A. (2003). Dynamin at the actin-membrane interface. *Curr. Opin. Cell Biol.* **15**, 31-39.
- Pasula, S., Cai, X., Dong, Y., Messa, M., McManus, J., Chang, B., Liu, X., Zhu, H., Mansat, R. S., Yoon, S. J. et al. (2012). Endothelial epsin deficiency decreases tumor growth by enhancing VEGF signaling. *J. Clin. Invest.* **122**, 4424-4438.
- Patterson, E. E., Minor, K. M., Tchernatynskaia, A. V., Taylor, S. M., Shelton, G. D., Ekenstedt, K. J. and Mickelson, J. R. (2008). A canine DNMI mutation is highly associated with the syndrome of exercise-induced collapse. *Nat. Genet.* **40**, 1235-1239.
- Pucadyil, T. J. and Schmid, S. L. (2008). Real-time visualization of dynamin-catalyzed membrane fission and vesicle release. *Cell* **135**, 1263-1275.
- Quan, A., McGeachie, A. B., Keating, D. J., van Dam, E. M., Rusak, J., Chau, N., Malladi, C. S., Chen, C., McCluskey, A., Cousin, M. A. et al. (2007). Myristyl trimethyl ammonium bromide and octadecyl trimethyl ammonium bromide are surface-active small molecule dynamin inhibitors that block endocytosis mediated by dynamin I or dynamin II. *Mol. Pharmacol.* **72**, 1425-1439.
- Raimondi, A., Ferguson, S. M., Lou, X., Armbruster, M., Paradise, S., Giovedi, S., Messa, M., Kono, N., Takasaki, J., Cappello, V. et al. (2011). Overlapping role of dynamin isoforms in synaptic vesicle endocytosis. *Neuron* **70**, 1100-1114.
- Robinson, M. S. (2004). Adaptable adaptors for coated vesicles. *Trends Cell Biol.* **14**, 167-174.
- Roux, A., Uyhazi, K., Frost, A. and De Camilli, P. (2006). GTP-dependent twisting of dynamin implicates constriction and tension in membrane fission. *Nature* **441**, 528-531.
- Saheki, Y. and De Camilli, P. (2012). Synaptic vesicle endocytosis. *Cold Spring Harb. Perspect. Biol.* **4**, a005645.
- Salazar, M. A., Kwiatkowski, A. V., Pellegrini, L., Cestra, G., Butler, M. H., Rossman, K. L., Serna, D. M., Sondek, J., Gertler, F. B. and De Camilli, P. (2003). Tuba, a novel protein containing bin/amphiphysin/Rvs and Dbl homology domains, links dynamin to regulation of the actin cytoskeleton. *J. Biol. Chem.* **278**, 49031-49043.
- Sawamiphak, S., Seidel, S., Essmann, C. L., Wilkinson, G. A., Pitulescu, M. E., Acker, T. and Acker-Palmer, A. (2010). Ephrin-B2 regulates VEGFR2 function in developmental and tumour angiogenesis. *Nature* **465**, 487-491.
- Schafer, D. A. (2004). Regulating actin dynamics at membranes: a focus on dynamin. *Traffic* **5**, 463-469.
- Schlunck, G., Damke, H., Kiessens, W. B., Rusk, N., Symons, M. H., Waterman-Storer, C. M., Schmid, S. L. and Schwartz, M. A. (2004). Modulation of Rac localization and function by dynamin. *Mol Biol Cell* **15**, 256-267.
- Schmid, S. L. and Frolov, V. A. (2011). Dynamin: functional design of a membrane fission catalyst. *Annu. Rev. Cell Dev. Biol.* **27**, 79-105.
- Shen, H., Ferguson, S. M., Dephoure, N., Park, R., Yang, Y., Volpicelli-Daley, L., Gygi, S., Schlessinger, J. and De Camilli, P. (2011). Constitutive activated Cdc42-associated kinase (Ack) phosphorylation at arrested endocytic clathrin-coated pits of cells that lack dynamin. *Mol. Biol. Cell* **22**, 493-502.
- Sousa, L. P., Lax, I., Shen, H., Ferguson, S. M., De Camilli, P. and Schlessinger, J. (2012). Suppression of EGFR endocytosis by dynamin depletion reveals that EGFR signaling occurs primarily at the plasma membrane. *Proc. Natl. Acad. Sci. USA* **109**, 4419-4424.
- Tanabe, K. and Takei, K. (2009). Dynamic instability of microtubules requires dynamin 2 and is impaired in a Charcot-Marie-Tooth mutant. *J. Cell Biol.* **185**, 939-948.
- Taylor, M. J., Lampe, M. and Merrifield, C. J. (2012). A feedback loop between dynamin and actin recruitment during clathrin-mediated endocytosis. *PLoS Biol.* **10**, e1001302.
- van der Blik, A. M. and Meyerowitz, E. M. (1991). Dynamin-like protein encoded by the Drosophila shibire gene associated with vesicular traffic. *Nature* **351**, 411-414.
- Wang, Y., Nakayama, M., Pitulescu, M. E., Schmidt, T. S., Bochenek, M. L., Sakakibara, A., Adams, S., Davy, A., Deutsch, U., Lüthi, U. et al. (2010). Ephrin-B2 controls VEGF-induced angiogenesis and lymphangiogenesis. *Nature* **465**, 483-486.
- Yamada, H., Abe, T., Li, S. A., Masuoka, Y., Isoda, M., Watanabe, M., Nasu, Y., Kumon, H., Asai, A. and Takei, K. (2009). Dynasore, a dynamin inhibitor, suppresses lamellipodia formation and cancer cell invasion by destabilizing actin filaments. *Biochem. Biophys. Res. Commun.* **390**, 1142-1148.
- Yamada, H., Abe, T., Satoh, A., Okazaki, N., Tago, S., Kobayashi, K., Yoshida, Y., Oda, Y., Watanabe, M., Tomizawa, K. et al. (2013). Stabilization of actin bundles by a dynamin 1/cortactin ring complex is necessary for growth cone filopodia. *J. Neurosci.* **33**, 4514-4526.
- Zhang, P. and Hinshaw, J. E. (2001). Three-dimensional reconstruction of dynamin in the constricted state. *Nat. Cell Biol.* **3**, 922-926.
- Zhang, J., Lawrance, G. A., Chau, N., Robinson, P. J. and McCluskey, A. (2008). From Spanish fly to room-temperature ionic liquids (RTILs): synthesis, thermal stability and inhibition of dynamin 1 GTPase by a novel class of RTILs. *New J. Chem.* **32**, 28-36.
- Züchner, S., Nouredine, M., Kennerson, M., Verhoeven, K., Claeys, K., De Jonghe, P., Merory, J., Oliveira, S. A., Speer, M. C., Stenger, J. E. et al. (2005). Mutations in the pleckstrin homology domain of dynamin 2 cause dominant intermediate Charcot-Marie-Tooth disease. *Nat. Genet.* **37**, 289-294.

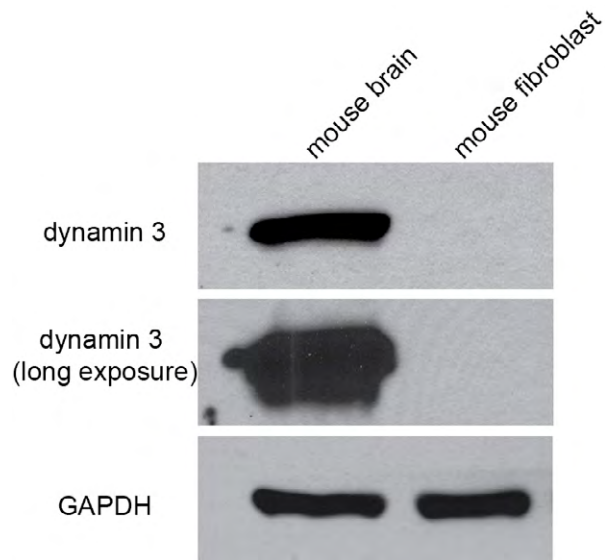


**Fig. S1. Very low expression levels of dynamin 3 in cultured mouse fibroblasts relative to its expression in mouse brain.** Lysates from wild-type mouse brain and fibroblasts were immunoblotted with an anti-dynamin 3 antibody. GAPDH is included as a loading control. Dynamin 3 is undetectable in the fibroblast sample, although it is detectable by mass spectrometry in these cells (see text).

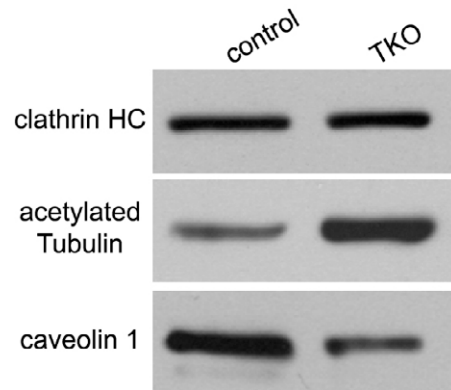


**Fig. S2. Altered caveolin and acetylated-tubulin levels in dynamin TKO cells.** Representative immunoblots of total cell homogenates from control and dynamin TKO cells. The anti-clathrin HC blot is included as a loading control.

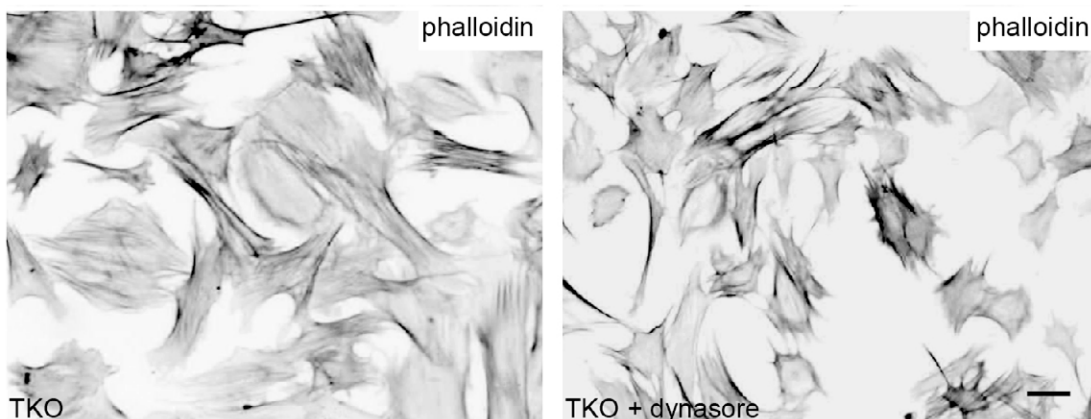


**Fig. S3. Dynasore affects cell morphology.** Fluorescent (AF594) phalloidin staining of fixed TKO cells incubated for 30 min at 37°C in the absence (left) or presence (right) of dynasore demonstrates dynasore-induced cell shrinkage. Scale bar=50  $\mu$ m.

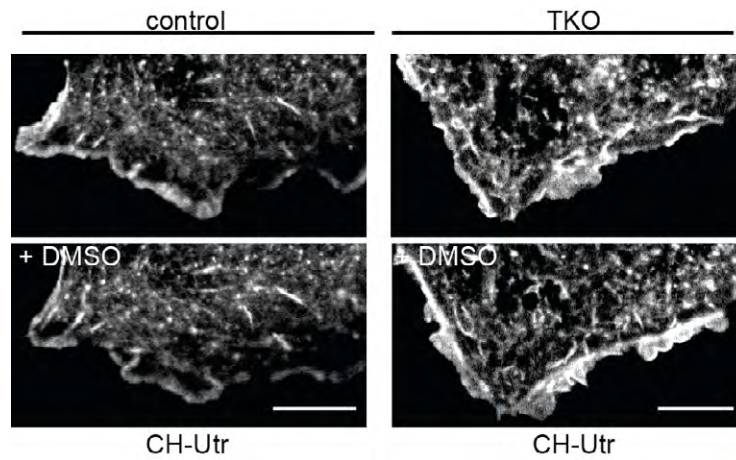
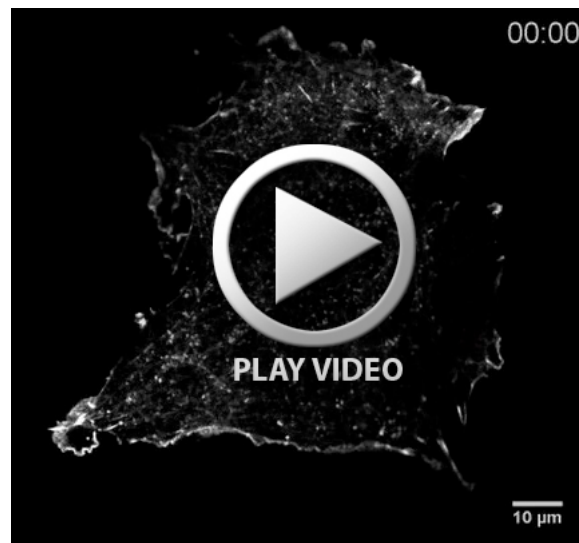


**Fig. S4. The concentration of DMSO present in the medium of dynasore-treated cells (DMSO is needed to solubilize dynasore) does not affect peripheral membrane ruffling in wild-type and dynamin TKO fibroblasts.** Fluorescence images of small regions of the cell periphery of a control (left) and a TKO cell (right) expressing CH-Utr fused to GFP. Cells were imaged before and after 20 min incubation with 0.15% DMSO by spinning disk confocal microscopy. Scale bar=10  $\mu$ m.



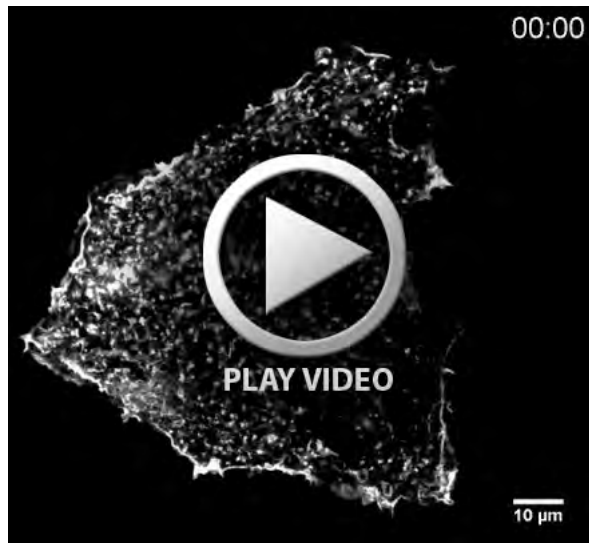
**Movie 1. Control cell expressing CH-Utr-GFP treated with DMSO**



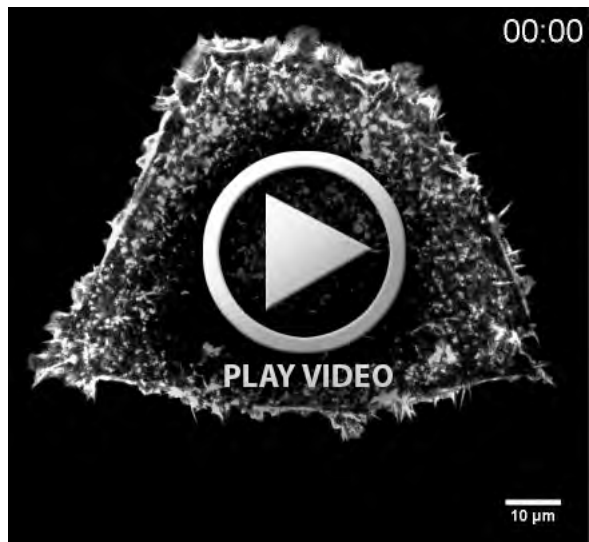
**Movie 2. Control cell expressing CH-Utr-GFP treated with dynasore**



**Movie 3. Control cell expressing CH-Utr-GFP treated with Dyngo-4a**



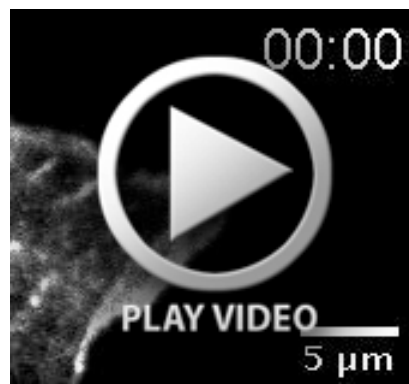
**Movie 4. Dynamin TKO cell expressing CH-Utr-GFP treated with DMSO**



**Movie 5. Dynamin TKO cell expressing CH-Utr-GFP treated with dynasore**



**Movie 6. Dynamin TKO cell expressing CH-Utr-GFP treated with Dyngo-4a**



**Movie 7. Cropped region of a control cell expressing CH-Utr-GFP treated with DMSO**



**Movie 8. Cropped region of a control cell expressing CH-Utr-GFP treated with dynasore**



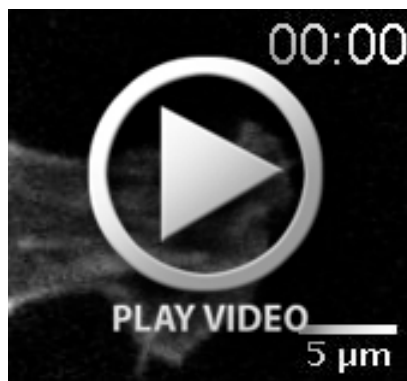
**Movie 9.** Cropped region of a control cell expressing CH-Utr-GFP treated with Dyngo-4a



**Movie 10.** Cropped region of a dynamin TKO cell expressing CH-Utr-GFP treated with DMSO



**Movie 11.** Cropped region of a dynamin TKO cell expressing CH-Utr-GFP treated with dynasore



**Movie 12.** Cropped region of a dynamin TKO cell expressing CH-Utr-GFP treated with Dyngo-4a